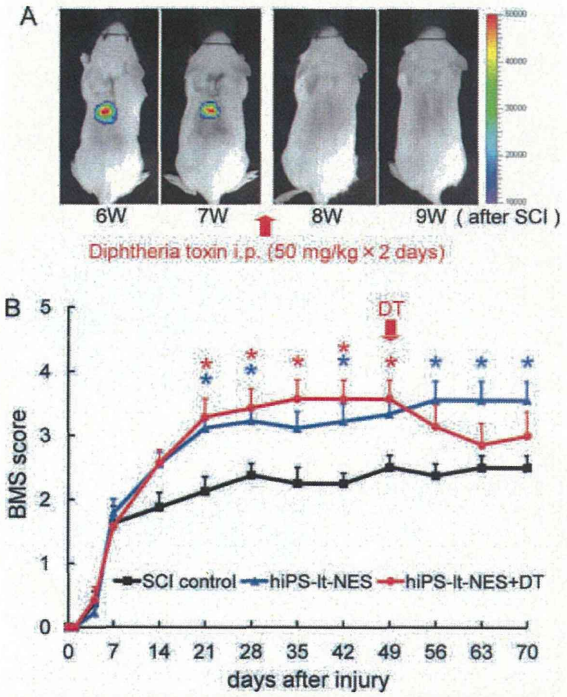

Figure 7. Transplanted cells contribute directly to the functional recovery of hind limb movement in SCI model mice. **(A):** Survival of transplanted cells was monitored using a bioluminescence imaging system. Seven weeks after SCI (6 weeks after transplantation), each mouse was administered DT. One week later, luciferase activity had completely disappeared in hiPS-lt-NES cell-transplanted mice. **(B):** Time course of functional recovery of hind limbs after SCI and DT administration. Data are means ± SEM (SCI control, $n = 8$; hiPS-lt-NES, $n = 9$; and hiPS-lt-NES+DT, $n = 7$). Hind limb function of hiPS-lt-NES cell-transplanted mice deteriorated after DT administration (red line). BMS values of the hiPS-lt-NES and hiPS-lt-NES+DT groups were compared with those of the SCI control group. *, $p < .05$. Abbreviations: BMS, Basso Mouse Scale; DT, diphtheria toxin; hiPS-lt-NES, human induced pluripotent stem cell-derived long-term self-renewing neuroepithelial-like stem; and SCI, spinal cord injury.

further improvements in the treatment of SCI [41]. However, transplantation studies of hiPS-NSCs, initially using mouse models of SCI [9], are in their infancy.

We have previously shown that human lt-NES cells, derived from different hESC and iPSC lines in two independent laboratories, exhibit consistent characteristics and retain their ability to proliferate and differentiate even after several passages and long-term in vitro growth [11]. In the present study, we investigated the differentiation potential of transplanted hiPS-lt-NES cells and found that the majority of differentiated hiPS-lt-NES cells in the injured spinal cord were neurons (Fig. 3D–3F), even though endogenous or transplanted NSCs in the injured spinal cord have been reported by others to differentiate preferentially into the glial lineage [42, 43]. Recent studies have indicated that neurons derived from transplanted human NSCs can integrate into the injured spinal cord and form synaptic connections with host neurons [33, 34]. We therefore took advantage of the tendency of our hiPS-lt-NES cells to differentiate into neurons and tried to apply these cells to reconstruction of the injured spinal cord.

Multiple therapeutic effects of NSC transplantation have been reported, and many different types of stem cells have been grafted into the injured spinal cord, yielding improved functional recovery in animal models [44, 45]. However, the growth of axons through the lesion to reinnervate the side caudal to the injury has so far been very limited. Our experiments using anterograde labeling of CST fibers revealed that this was also the case after transplantation of hiPS-lt-NES cells (Fig. 4). We have previously shown that neurons derived from mouse NSCs could restore disrupted neuronal circuits [15]. Consistent with that observation, we demonstrated here that WGA-positive cell numbers in hiPS-lt-NES cell-treated mice were higher than those in SCI control mice in the area caudal to the SCI (Fig. 5A, 5B). Furthermore, immunohistochemistry using species-specific antibodies for presynaptic markers suggested that transplant-derived neurons made synapses with endogenous neurons (Fig. 5C-2, 5C-2′, 5C-3, and 5C-3′). These results suggest that WGA was transferred to the caudal area through the lesion site via new synaptic connections, and that hiPS-lt-NES cell transplantation promoted CST reconstruction in a relay fashion. Other studies have provided evidence that local neurons can form intraspinal neural circuits in the lesion site and make synaptic connections with descending-tract collaterals after SCI [32, 46], and human NSCs transplanted into the injured rat or mouse spinal cord differentiated into neurons that formed axons and synapses, and also established contacts with host neurons [4, 34].

As well as their roles in cell replacement, NSCs reportedly exert other effects through the secretion of neurotrophic factors [37], which, by means such as suppressing myelin inhibitors, prevent neuronal cell death, enhance remyelination and regenerate axons [47, 48]. We found that transplantation of hiPS-lt-NES cells supported the survival of endogenous neurons (Fig. 6). Conversely, ablation of transplanted cells decreased previously attained functional recovery (Fig. 7), suggesting that transplanted cells contribute directly to functional recovery of hind limb movement in SCI model mice. In summary, we suggest that not only neurons derived from transplanted hiPS-lt-NES cells but also surviving endogenous neurons contribute to functional improvement by forming multiple synaptic connections which restore disrupted neuronal circuits.

Following injury, demyelinated and reconstructed axons must be remyelinated to ensure proper functional recovery. Generally, endogenous or transplanted NSCs which differentiate into oligodendrocytes have been reported to contribute to remyelination of axons and thereby to help in recovery after SCI. Transplanted oligodendrocyte progenitor cells (OPCs) derived from human ESCs have been shown to differentiate into oligodendrocytes and enhance remyelination in the moderate rat model of contusion spinal cord injury [5, 6]. A further study reported that in complete spinal cord transection rats, locomotor recovery after transplantation with both OPCs and human ESC-derived motor neuron progenitor cells was significantly greater than after treatment with either cell type alone [49]. Given that the application of stem cells and their progenitors for transplantation is currently in its infancy, and that SCI pathology differs between contusion and transection [50], these findings indicate that neural cells in an appropriate lineage should be transplanted according to the degree and/or type of SCI.

When ES and iPS cells are used for transplantation treatment, a key consideration is the likelihood of tumor formation, since the transplanted cell population may include undifferentiated cells [51, 52]. Indeed, the sources and methods of induction of NSCs are critical for differentiation and tumor formation [33, 53]. Neurosphere cultures are heterogeneous and sensitive to variations in methodological procedures [12], whereas monolayer cell cultures give rise to more homogeneous population [13, 14]. In this study, we detected no tumor

formation in more than 40 hiPS-lt-NES cell-treated mice up to 12 weeks after SCI. This is probably attributable to complete differentiation of hiPS cells into NES cells in our robust and stable monolayer cell cultures, since the NES cells were established by initially purifying neural rosette structures from differentiating cultures [11]. Furthermore, we transplanted hiPS-lt-NES cells which had been expanded in the presence of growth factors and passaged more than 20 times. Before human iPS cell-based therapies can be implemented for clinical application, the cells' proliferation and tumor formation after transplantation must be strictly evaluated.

Conclusion

In this study, we have demonstrated that hiPS-lt-NES cells survived and differentiated in the injured spinal cord of NOD-SCID mice, and promoted functional recovery of hind limbs. Moreover, we have shown that transplanted hiPS-lt-NES cells support the reconstruction of CST pathways, promote endogenous neuron survival, and directly contribute to improved hind limb movement. To achieve a more efficient treatment for SCI, detailed investigations of hiPS-lt-NES cells and SCI pathology will be necessary. Nevertheless, our study raises the possibility that hiPS-based therapy can be applied in the near future to SCI patients who currently have few or no therapeutic options.

Acknowledgments

We thank M. Saito and K. Kohno for providing diphtheria toxin, H. Miyoshi, H. J. Okano, and H. Okano for lentiviral vectors, Y. Yoshihara for WGA-expressing adenovirus, N. Uchida for anti-human specific antibodies, and S. Nori and M. Nakamura for species-specific antibodies. We also thank Y. Bessho, T. Matsui, Y. Nakahata, T. Matsuda, S. Komai, and M. Arai for valuable discussions and technical advice, T. Matta for statistical analysis, I. Smith for editing the manuscript, and M. Tano for secretarial assistance. lt-NES® is a registered trademark of LIFE & BRAIN GmbH, Bonn, Germany.

Disclosure of Potential Conflicts of Interest

The authors indicate no potential conflicts of interest.

References

1 Ditunno JF, Formal CS. Chronic spinal cord injury. N Engl J Med 1994;330:550–556.
2 Ogawa Y, Sawamoto K, Miyata T et al. Transplantation of in vitro-expanded fetal neural progenitor cells results in neurogenesis and functional recovery after spinal cord contusion injury in adult rats. J Neurosci Res 2002;69:925–933.
3 Iwanami A, Kaneko S, Nakamura M et al. Transplantation of human neural stem cells for spinal cord injury in primates. J Neurosci Res 2005;80:182–190.
4 Cummings BJ, Uchida N, Tamaki SJ et al. Human neural stem cells differentiate and promote locomotor recovery in spinal cord-injured mice. Proc Natl Acad Sci USA 2005;102:14069–14074.
5 Keirstead HS, Nistor G, Bernal G et al. Human embryonic stem cell-derived oligodendrocyte progenitor cell transplants remyelinate and restore locomotion after spinal cord injury. J Neurosci 2005;25:4694–4705.
6 Sharp J, Frame J, Siegenthaler M et al. Human embryonic stem cell-derived oligodendrocyte progenitor cell transplants improve recovery after cervical spinal cord injury. Stem Cells 2010;28:152–163.
7 Takahashi K, Yamanaka S. Induction of pluripotent stem cells from mouse embryonic and adult fibroblast cultures by defined factors. Cell 2006;126:663–676.
8 Takahashi K, Tanabe K, Ohnuki M et al. Induction of pluripotent stem cells from adult human fibroblasts by defined factors. Cell 2007;131:861–872.
9 Nori S, Okada Y, Yasuda A et al. Grafted human-induced pluripotent stem-cell-derived neurospheres promote motor functional recovery after spinal cord injury in mice. Proc Natl Acad Sci USA 2011;108:16825–16830.
10 Koch P, Opitz T, Steinbeck JA et al. A rosette-type, self-renewing human ES cell-derived neural stem cell with potential for in vitro instruction and synaptic integration. Proc Natl Acad Sci USA 2009;106:3225–3230.
11 Falk A, Koch P, Kesavan J et al. Capture of neuroepithelial-like stem cells from pluripotent stem cells provides a versatile system for in vitro production of human neurons. PLoS One 2012;7:e29597.
12 Kim HT, Kim IS, Lee IS et al. Human neurospheres derived from the fetal central nervous system are regionally and temporally specified but are not committed. Exp Neurol 2006;199:222–235.
13 Conti L, Pollard SM, Gorba T et al. Niche-independent symmetrical self-renewal of a mammalian tissue stem cell. PLoS Biol 2005;3:e283.
14 Pollard SM, Conti L, Sun Y et al. Adherent neural stem (NS) cells from fetal and adult forebrain. Cereb Cortex 2006;16 Suppl 1:i112–i120.
15 Abematsu M, Tsujimura K, Yamano M et al. Neurons derived from transplanted neural stem cells restore disrupted neuronal circuitry in a mouse model of spinal cord injury. J Clin Invest 2010;120:3255–3266.
16 Sun Y, Pollard S, Conti L et al. Long-term tripotent differentiation capacity of human neural stem (NS) cells in adherent culture. Mol Cell Neurosci 2008;38:245–258.
17 Miyoshi H, Blömer U, Takahashi M et al. Development of a self-inactivating lentivirus vector. J Virol 1998;72:8150–8157.
18 Okada S, Ishii K, Yamane J et al. In vivo imaging of engrafted neural stem cells: Its application in evaluating the optimal timing of transplantation for spinal cord injury. FASEB J 2005;19:1839–1841.
19 Basso DM, Fisher LC, Anderson AJ et al. Basso Mouse Scale for locomotion detects differences in recovery after spinal cord injury in five common mouse strains. J Neurotrauma 2006;23:635–659.
20 Setoguchi T, Nakashima K, Takizawa T et al. Treatment of spinal cord injury by transplantation of fetal neural precursor cells engineered to express BMP inhibitor. Exp Neurol 2004;189:33–44.
21 Hata K, Fujitani M, Yasuda Y et al. RGMa inhibition promotes axonal growth and recovery after spinal cord injury. J Cell Biol 2006;173:47–58.
22 Kaneko S, Iwanami A, Nakamura M et al. A selective Sema3A inhibitor enhances regenerative responses and functional recovery of the injured spinal cord. Nat Med 2006;12:1380–1389.
23 Pronichev IV, Lenkov DN. Functional mapping of the motor cortex of the white mouse by a microstimulation method. Neurosci Behav Physiol 1998;28:80–85.
24 Yoshihara Y, Mizuno T, Nakahira M et al. A genetic approach to visualization of multisynaptic neural pathways using plant lectin transgene. Neuron 1999;22:33–41.
25 Kinoshita N, Mizuno T, Yoshihara Y. Adenovirus-mediated WGA gene delivery for transsynaptic labeling of mouse olfactory pathways. Chem Senses 2002;27:215–223.
26 Furukawa N, Saito M, Hakoshima T et al. A diphtheria toxin receptor deficient in epidermal growth factor-like biological activity. J Biochem 2006;140:831–841.
27 Saito M, Iwawaki T, Taya C et al. Diphtheria toxin receptor-mediated conditional and targeted cell ablation in transgenic mice. Nat Biotechnol 2001;19:746–750.
28 Luchetti S, Beck KD, Galvan MD et al. Comparison of immunopathology and locomotor recovery in C57BL/6, BUB/BnJ, and NOD-SCID mice after contusion spinal cord injury. J Neurotrauma 2010;27:411–421.
29 Yan J, Welsh AM, Bora SH et al. Differentiation and tropic/trophic effects of exogenous neural precursors in the adult spinal cord. J Comp Neurol 2004;480:101–114.
30 Nothias JM, Mitsui T, Shumsky JS et al. Combined effects of neurotrophin secreting transplants, exercise, and serotonergic drug challenge improve function in spinal rats. Neurorehabil Neural Repair 2005;19:296–312.
31 Kim D, Murray M, Simansky KJ. The serotonergic 5-HT(2C) agonist *m*-chlorophenylpiperazine increases weight-supported locomotion without development of tolerance in rats with spinal transections. Exp Neurol 2001;169:496–500.

32 Courtine G, Song B, Roy RR et al. Recovery of supraspinal control of stepping via indirect propriospinal relay connections after spinal cord injury. Nat Med 2008;14:69–74.
33 Hooshmand MJ, Sontag CJ, Uchida N et al. Analysis of host-mediated repair mechanisms after human CNS-stem cell transplantation for spinal cord injury: Correlation of engraftment with recovery. PLoS One 2009;4:e5871.
34 Yan J, Xu L, Welsh AM et al. Extensive neuronal differentiation of human neural stem cell grafts in adult rat spinal cord. PLoS Med 2007;4:e39.
35 Nakamura M, Houghtling RA, MacArthur L et al. Differences in cytokine gene expression profile between acute and secondary injury in adult rat spinal cord. Exp Neurol 2003;184:313–325.
36 Bareyre FM, Schwab ME. Inflammation, degeneration and regeneration in the injured spinal cord: insights from DNA microarrays. Trends Neurosci 2003;26:555–563.
37 Lu P, Tuszynski MH. Growth factors and combinatorial therapies for CNS regeneration. Exp Neurol 2008;209:313–320.
38 Okita K, Nakagawa M, Hyenjong H et al. Generation of mouse induced pluripotent stem cells without viral vectors. Science 2008; 322:949–953.
39 Zhou H, Wu S, Joo JY et al. Generation of induced pluripotent stem cells using recombinant proteins. Cell Stem Cell 2009;4:381–384.
40 Kaji K, Norrby K, Paca A et al. Virus-free induction of pluripotency and subsequent excision of reprogramming factors. Nature 2009;458: 771–775.
41 Lindvall O, Kokaia Z. Stem cells in human neurodegenerative disorders–time for clinical translation? J Clin Invest 2010;120:29–40.
42 Cao QL, Howard RM, Dennison JB et al. Differentiation of engrafted neuronal-restricted precursor cells is inhibited in the traumatically injured spinal cord. Exp Neurol 2002;177:349–359.
43 Han SS, Kang DY, Mujtaba T et al. Grafted lineage-restricted precursors differentiate exclusively into neurons in the adult spinal cord. Exp Neurol 2002;177:360–375.
44 Louro J, Pearse DD. Stem and progenitor cell therapies: recent progress for spinal cord injury repair. Neurol Res 2008;30:5–16.
45 Jain KK. Cell therapy for CNS trauma. Mol Biotechnol 2009;42: 367–376.
46 Bareyre FM, Kerschensteiner M, Raineteau O et al. The injured spinal cord spontaneously forms a new intraspinal circuit in adult rats. Nat Neurosci 2004;7:269–277.
47 Shumsky JS, Tobias CA, Tumolo M et al. Delayed transplantation of fibroblasts genetically modified to secrete BDNF and NT-3 into a spinal cord injury site is associated with limited recovery of function. Exp Neurol 2003;184:114–130.
48 Tobias CA, Shumsky JS, Shibata M et al. Delayed grafting of BDNF and NT-3 producing fibroblasts into the injured spinal cord stimulates sprouting, partially rescues axotomized red nucleus neurons from loss and atrophy, and provides limited regeneration. Exp Neurol 2003;184: 97–113.
49 Erceg S, Ronaghi M, Oria M et al. Transplanted oligodendrocytes and motoneuron progenitors generated from human embryonic stem cells promote locomotor recovery after spinal cord transection. Stem Cells 2010;28:1541–1549.
50 Siegenthaler MM, Tu MK, Keirstead HS. The extent of myelin pathology differs following contusion and transection spinal cord injury. J Neurotrauma 2007;24:1631–1646.
51 Miura K, Okada Y, Aoi T et al. Variation in the safety of induced pluripotent stem cell lines. Nat Biotechnol 2009;27:743–745.
52 Tsuji O, Miura K, Okada Y et al. Therapeutic potential of appropriately evaluated safe-induced pluripotent stem cells for spinal cord injury. Proc Natl Acad Sci USA 2010;107:12704–12709.
53 Jensen JB, Parmar M. Strengths and limitations of the neurosphere culture system. Mol Neurobiol 2006;34:153–161.

See www.StemCells.com for supporting information available online.

1C3-3

現実およびバーチャルリアリティ空間におけるマウスの肢刺激を手掛かりとした弁別課題の確立

本間千尋[1)]、山田一之[1)]、鴨志田敦史[1,2)]、茂泉俊次郎[1,3)]、鮫島正大[1,3)]、織田充[1)]、山川宏[1)]、○村山正宜[1)]

(1) 理研 BSI 行動神経生理、2) 日本ナショナルインスツルメンツ、3) ソリッドレイ研究所)

New experimental systems for a tactile discrimination task in real and virtual world

Chihiro Homma[1)], Kazuyuki Yamada[1)], Atsushi Kamoshida[1,2)], Shunjiro Moizumi[1,3)], Masahiro Samejima[1,3)], Mitsuru Oda[1)], Hiroshi Yamakawa[1)], * Masanori Murayama[1)]

(1)Lab for Behav Neurophysiol, BSI, RIKEN, 2) National Instruments Japan Corporation, 3) Solidray Corporation)

Abstract— Cutaneous sensations are thought to be represented in primary somatosensory cortex (S1) as a result of neural activity, which can then be used for higher brain functions such as decision-making, attention, and memory. In a previous study we showed that the intensity of limb stimulation in rodents is coded by the dendritic activity of layer 5 pyramidal neurons in S1. This implies that somatosensation of tactile stimuli can also be used as a primary mode of input that is sent to higher brain areas. To further test this hypothesis, we developed a new experimental system in which mice discriminated texture in a modified Y-maze; from these results, we are now applying this task in virtual world situations.

Key Words: somatosensation, discrimination, Y-maze

1 はじめに

体性感覚は空間や環境を認知するにあたり大きな役割を担っている。特にげっ歯類が環境を認知する際は体性感覚情報に強く依存しており、この特性を利用した学習や意思決定等を含んだ高次脳機能の神経科学的な解明を試みた研究が昨今多く報告されている[1,2)]。しかしいまだその神経メカニズムは未知の部分が多い。そこで本研究では、マウス自由行動下にて体性感覚情報が高次脳領域へ到達するまでの神経回路を解明することを目的として、体性感覚刺激を手がかりとした弁別課題の実施可能な自動化 Y 迷路装置を作成した。本装置はすべて自動化されており、電気生理学などの他の技術的手法を合わせて使用しやすくまた動物を用いた学習訓練に特有の実験者への負担を軽減することもできる。

一方、脳機能の神経科学的アプローチの一つの手法として、脳のイメージング法があるが、二光子顕微鏡などの大型装置を使用したイメージングを行うためには頭部固定化で実験を行う必要があり、そのため VR システムの搭載が便利であり昨今広く使用されている[3,4)]。我々は現実空間における Y 迷路課題の訓練結果に基づいてバーチャルリアリティ (VR) 空間における Y 迷路課題の確立を試みており、ここにその進捗を報告する。

2 現実空間における Y 迷路課題

2.1 装置および実験方法

本装置は通常の Y 迷路とは異なり終点と始点が連結した形状をしている。また試行開始および終了時に開閉する扉と触覚呈示部分、加えて報酬取得部分がすべて自動化されている。さらに自動化部分はすべてソフトウェア (LabVIEW 2011 ver.11, National Instruments) で制御されており、学習が成立するまでの一連の訓練を自動で行うことができ、手技の統一および時間や手間の効率化をはかることができる (Fig. 1)。

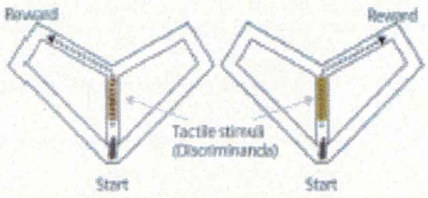

Fig.1: Automated Y-maze

マウスは 6 週齢以降の C57BL/6J (日本 SLC) 系統を用いた。訓練は床に設置された触覚刺激 (紙やすり #40 または厚紙) 通過後、正解方向を選択した場合は報酬個所で報酬が得られ、不正解方向を選択した場合は得ることができない、継時弁別訓練法を用いた。

2.2 結果

訓練は各マウスで 30 試行 1 セッションを 1 日に 1 回行った。訓練が重なるにつれマウスは徐々に装置の特性をつかみ、報酬獲得後すぐに開始部分に戻るようになる (Fig. 2)。訓練は初めに一種類の触覚刺激と

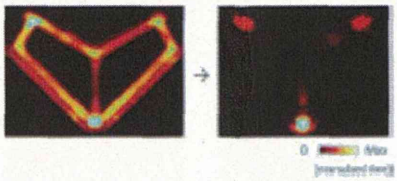

Fig. 2: Representative data sample of time spent duration of mouse's location during the training

SY0014/12/0000-0114 © 2012 SICE

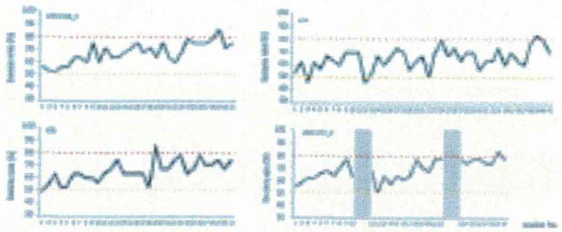

Fig. 3: Learning curve of discrimination training
Red dashed line; 80% of success rate, Yellow dashed line; chance level, Gray zone; rest period of training

それに対応する片一方向の連合学習を形成させ、両刺激の学習獲得が確認できた後、準無作為に刺激を呈示しさらに訓練を続けた。その結果、現在のところ 5 匹のマウスで約 80%の正解率を示した。Fig. 3 に4個体の正解率の推移を示した。

3 VR 空間における Y 迷路課題

3.1 装置および実験方法

開発した VR システムはマウスの水平視野を 270 度覆う円柱様型のスクリーンと一軸式回転型の回し車、報酬供給装置から構成される。VR 環境はソフトウェア（OmegaSpace ver.3.2, Solidray. Co.）を使用して作成した。また回し車には制御可能な触覚呈示部分が存在し、VR 環境と回し車および触覚呈示部分の動作、報酬供給装置はすべてソフトウェア (LabVIEW 2011 ver.11)で制御可能とし、本装置も一連の訓練を自動で行うことができる（Fig. 4）。マウスの進行方向はマウスの頭部と体の重心の角度より決定した。

使用したマウスの条件は前述と同様であり、訓練前に頭部固定化で行うためチタン製ヘッドプレートを接着した。訓練は初めに VR 空間に馴致するため直線走路課題を行い、一定距離走行することで報酬を得ることのできる道具的条件付けを行った。潤滑な走行を確認した後、VR-Y 迷路課題に移行した（Fig. 5）。

3.2 結果

訓練は各マウスで 30 試行 1 セッションを 1 日に 1 回行った。直線走路課題開始時は進行方向を決定する角度情報の分散が大きく、訓練が進むにつれ分散が小さくなり、1 セッションあたりの平均回転速度も大

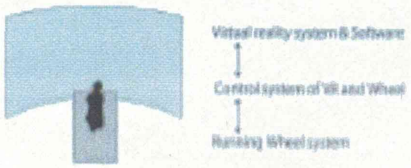

Fig. 4: VR system

Fig. 5: Y-maze in VR world
Picture before the branch point

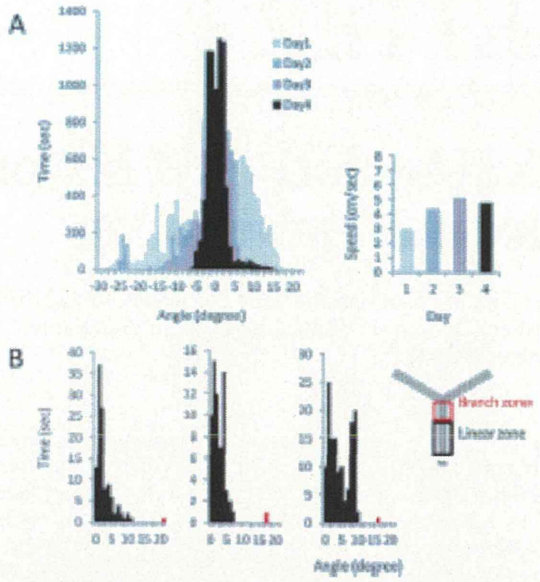

Fig. 6: Representative data sample of accustomising to virtual tracks. B: Each graph represents angle (absolute value) in a trial. Black bar; Range of angle at linear track in Y-maze, Red bar; Maximum angle at branch zone

きくなった（Fig. 6A）。開始時は VR 空間および回し車上の走行に馴致が見られないが、訓練が進むにつれ、いずれにも馴致できたことが示唆される。

VR-Y 迷路課題では Y 迷路分岐部分通過後報酬を与える行動の形成を行ったが、呈示された分岐部分に合わせて体の角度を大きくし左右方向に進もうとするような行動が確認された（Fig. 6B）。

4 まとめ

我々は自動化 Y 迷路を作成し訓練を行うことで、マウスを用いた触覚弁別課題を確立することできた。さらに、その課題を VR 空間内で行えるシステムを構築し、訓練後マウスが VR 空間に準じて動きを変えることが示唆される結果を確認できた。今後は自動化触覚刺激を呈示し弁別課題を試みる予定である。また本両システムを使用し、光遺伝学的手法や電気生理学的手法を用いた脳機能解明へのアプローチを目指し現在準備を進めている。

参考文献

1) Petreanu L, Gutnisky DA, Huber D, Xu NL, O'Connor DH, Tian L, Looger L, Svoboda K.: Activity in motor-sensory projections reveals distributed coding in somatosensation., Nature, 489(7415), 299/303 (2012)
2) Maricich S.M, Morrison K.M, Mathes E.L, Brewer B.M.: Rodents rely on Merkel cells for texture discrimination tasks., J Neurosci. 32(10), 3296/3300 (2012)
3) Harvey CD, Collman F, Dombeck DA, Tank DW.: Intracellular dynamics of hippocampal place cells during virtual navigation., Nature, 461(7266), 941/946 (2009)
4) Youngstrom IA, Strowbridge BW.: Visual landmarks facilitate rodent spatial navigation in virtual reality environments., Learn Mem., 19(3), 84/90 (2012)

LETTER

doi:10.1038/nature10656

GlcNAcylation of histone H2B facilitates its monoubiquitination

Ryoji Fujiki[1], Waka Hashiba[1], Hiroki Sekine[1], Atsushi Yokoyama[1], Toshihiro Chikanishi[1], Saya Ito[1], Yuuki Imai[1], Jaehoon Kim[2], Housheng Hansen He[3], Katsuhide Igarashi[4], Jun Kanno[4], Fumiaki Ohtake[1], Hirochika Kitagawa[1], Robert G. Roeder[2], Myles Brown[3] & Shigeaki Kato[1,5]

Chromatin reorganization is governed by multiple post-translational modifications of chromosomal proteins and DNA[1,2]. These histone modifications are reversible, dynamic events that can regulate DNA-driven cellular processes[3,4]. However, the molecular mechanisms that coordinate histone modification patterns remain largely unknown. In metazoans, reversible protein modification by *O*-linked *N*-acetylglucosamine (GlcNAc) is catalysed by two enzymes, *O*-GlcNAc transferase (OGT) and *O*-GlcNAcase (OGA)[5,6]. However, the significance of GlcNAcylation in chromatin reorganization remains elusive. Here we report that histone H2B is GlcNAcylated at residue S112 by OGT *in vitro* and in living cells. Histone GlcNAcylation fluctuated in response to extracellular glucose through the hexosamine biosynthesis pathway (HBP)[5,6]. H2B S112 GlcNAcylation promotes K120 monoubiquitination, in which the GlcNAc moiety can serve as an anchor for a histone H2B ubiquitin ligase. H2B S112 GlcNAc was localized to euchromatic areas on fly polytene chromosomes. In a genome-wide analysis, H2B S112 GlcNAcylation sites were observed widely distributed over chromosomes including transcribed gene loci, with some sites co-localizing with H2B K120 monoubiquitination. These findings suggest that H2B S112 GlcNAcylation is a histone modification that facilitates H2BK120 monoubiquitination, presumably for transcriptional activation.

Some nuclear proteins have been shown to be GlcNAcylated by OGT, for example the enzymatic activity of histone H3K4 methyltransferase 5 (MLL5) is modulated by GlcNAcylation[7–9]. To identify chromatin substrates for OGT further, we screened for unknown GlcNAcylated glycoproteins in HeLa cell chromatin. GlcNAcylated proteins were purified by WGA lectin column chromatography and anti-GlcNAc antibody (clone RL2). Liquid chromatography–mass spectrometry (LC–MS)/MS analysis of the fraction revealed 284 factors, including previously reported GlcNAcylated glycoproteins[6,10] (Supplementary Table 1). Among the candidates, the enrichment of nucleosomes was confirmed by silver staining and western blotting (Supplementary Fig. 2), suggesting one or more histone(s) might have been GlcNAcylated. As OGT is the only known nuclear enzyme for protein GlcNAcylation[5], we asked whether histones served as substrates for OGT *in vitro* (Supplementary Fig. 3). H2A and H2B, as well as H2A variants (H2A.X and H2A.Z), but not H3 and H4, appeared to be GlcNAcylated (Fig. 1a). With histone octamers, H2B, but not H2A, appeared to serve as a substrate (Fig. 1b). Likewise, H2B in *Drosophila* histone was also GlcNAcylated (Supplementary Fig. 4), implying that H2B GlcNAcylation is conserved in metazoans.

A quadrupole (Q)-time of flight (TOF) MS assessment of the *in vitro* GlcNAcylated H2B showed that OGT could transfer three GlcNAc moieties to H2B (Supplementary Fig. 5). Electro-transfer-dissociation (ETD)–MS/MS mapped the sites to S91, S112 and S123 (Fig. 1c and Supplementary Fig. 6). Unlike a recent report[11], we were unable to detect the reported sites in H2B S36 and H4 S47. However, H2A T101 was detected as a GlcNAc site when H2A protein alone was used (data not shown). This discrepancy in identified GlcNAc sites might be due to differences in experimental approaches.

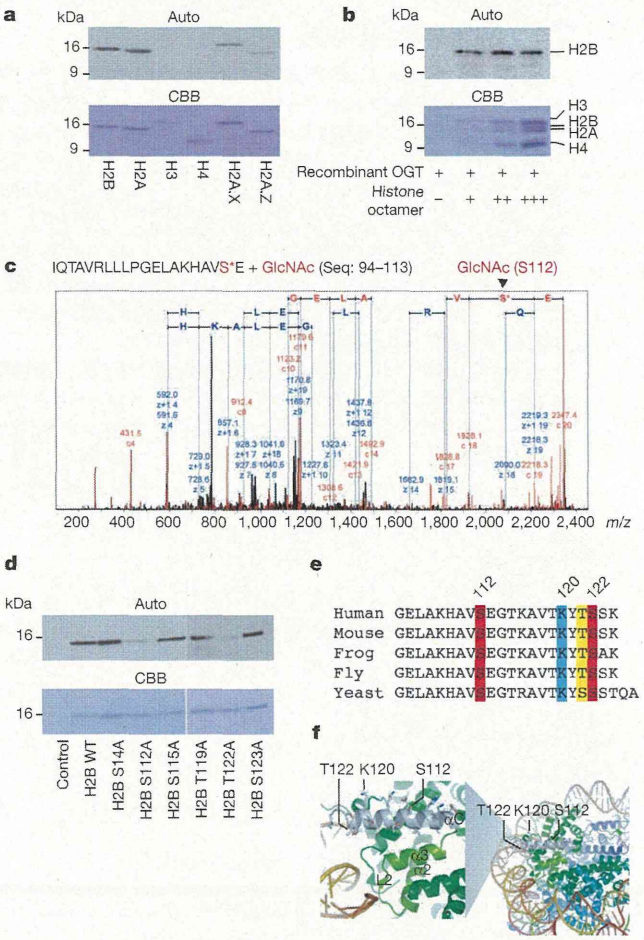

Figure 1 | H2B is GlcNAcylated at the C-terminal S112. a, **b**, *In vitro* OGT assay with recombinant histones (**a**) or the octamers reconstituted *in vitro* (**b**). Histones were GlcNAcylated by uridine diphosphate (UDP)-[^{3}H]GlcNAc and OGT, and the radiolabelled histones were subjected to autoradiography (top) and CBB staining (bottom). **c**, ETD–MS/MS scanned the GlcNAcylated peptides (2349.43 *m*/*z*) in Supplementary Fig. 5b. **d**, A series of H2B mutants at the indicated S/T was assessed by *in vitro* OGT assays. **e**, Sequence alignment of αC. **f**, The locations of the GlcNAc sites and the ubiquitination site of H2B in a nucleosome. The αC helix is illustrated as a white ribbon.

[1]Institute of Molecular and Cellular Biosciences, University of Tokyo, 1-1-1 Yayoi, Bunkyo-ku, Tokyo 113-0032, Japan. [2]Laboratory of Biochemistry and Molecular Biology, The Rockefeller University, New York, New York 10065, USA. [3]Department of Medical Oncology, Dana-Farber Cancer Institute and Harvard Medical School, Boston, Massachusetts 02115, USA. [4]Division of Cellular and Molecular Toxicology, National Institute of Health Sciences, 1-18-1 Kamiyoga, Setagaya-ku, Tokyo 158-8501, Japan. [5]ERATO, Japan Science and Technology Agency, Kawaguchi, Saitama 332-0012, Japan.

Next, *in vitro* OGT assays using peptide arrays covering full-length H2B revealed peaks at 101–115 peptides in the carboxy (C)-terminal α-helix (αC)[12] (Supplementary Fig. 7). This peptide was found to bear only one moiety by matrix-assisted laser desorption/ionization–time of flight (MALDI–TOF)/MS (Supplementary Fig. 8). Indeed, substitutions of S112 and T122 to A significantly reduced *in vitro* GlcNAcylation by OGT (Fig. 1d), but not mutations in the amino (N)-terminal tail (Supplementary Fig. 9). On the basis of these data, we concluded that the conserved S112 was a GlcNAc site in H2B, whereas T122 might be needed for recognition by OGT (Fig. 1e, f).

With our newly developed antibody (Supplementary Fig. 10), H2B S112 GlcNAc was detected in histones of HeLa cells. Depletion of glucose from the media for 24 h induced deglycosylation with neither overt cell death (Fig. 2a and Supplementary Fig. 11) nor alteration in histone acetylation marks of cell state indicators (H3 K14, H3 K56, H4 K16)[13,14] (Supplementary Fig. 12). H2B S112 GlcNAc could be restored by re-treatment with glucose at physiological concentrations (Supplementary Fig. 13).

Because many histone modifications are orchestrated, we tested if H2B S112 GlcNAc influenced H2B K120 monoubiquitination because of their proximity. After glucose depletion, replenishment of glucose gradually increased global GlcNAcylation of proteins, followed by H2B S112 GlcNAc and H2B monoubiquitination (Fig. 2b, c). Their reciprocal modifications disappeared when OGT was knocked down (Fig. 2d and Supplementary Fig. 14). In addition, in the immunoprecipitates of H2B containing the S112A and T122A double mutations (H2B AA), no response of K120 monoubiquitination to extracellular glucose was detected (Fig. 2e and Supplementary Fig. 15). Conversely, GlcNAcylation of H2B S112 was observed, even when K120 was mutated to R (Fig. 2e). From these findings, we conclude that H2B K120 monoubiquitination is mediated, at least in part, through S112 GlcNAcylation.

As glucosamine, but not pyruvate, potentiated H2B S112 GlcNAc (Fig. 2f), it appeared that this GlcNAcylation step was dependent on the HBP. To clarify this point, two HBP inhibitors (DON and AZA) were tested (Supplementary Information). After glucose depletion from media, these inhibitors attenuated the effect of glucose in H2B S112 GlcNAcylation along with K120 monoubiquitination (Fig. 2f).

In yeast, it was previously shown that H2B K120 monoubiquitination was induced by carbohydrates by glycolysis[15]. To address this issue, inhibitors of both glycolysis and deGlcNAcylation were applied to assess the crosstalk between the two modifications. When the cells were treated with iodoacetate, which blocks glycolysis but not HBP[15], the glucose effects on histone modifications were impaired, whereas the additional treatment of an OGA inhibitor (PUGNAc) restored both H2B S112 and K120 monoubiquitination (Supplementary Fig. 16). These data support the notion that H2B S112 GlcNAc senses decreases in glucose levels below normal levels and acts to promote H2B monoubiquitination, a modification that is associated with active transcription. Together with the fact that OGT is absent in yeast[6], the present H2B S112 GlcNAc-dependent pathway appears to constitute a system capable of sensing nutritional states in metazoans.

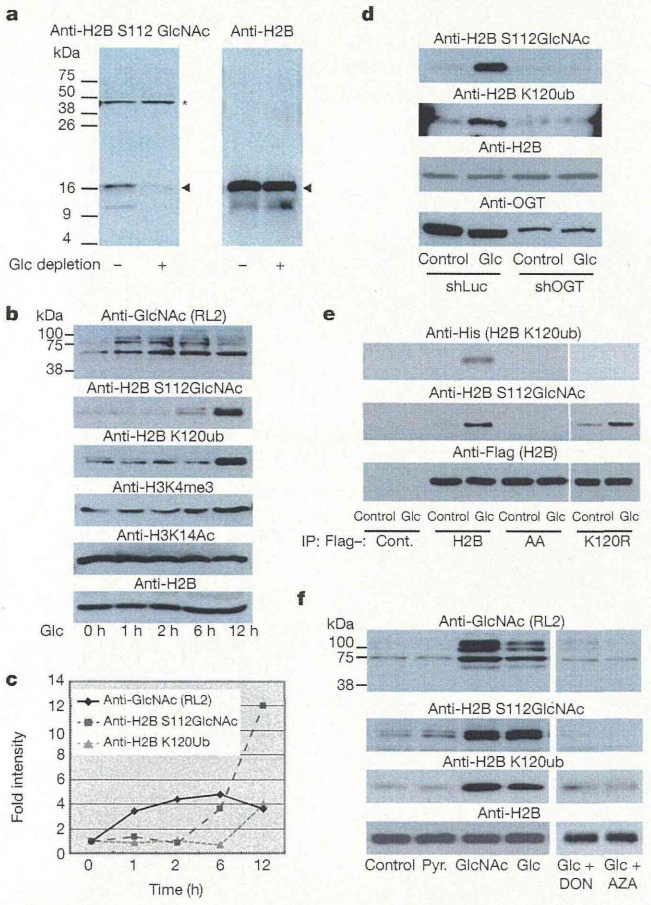

Figure 2 | H2B S112 GlcNAc is a glucose-responsive modification linked to K120 monoubiquitination (ub). **a**, Chromatin was prepared from HeLa cells cultured in media with or without 1 g l^{-1} glucose (Glc) for 24 h, and subjected to western blotting. Arrowheads show the indicated proteins. Asterisks indicate non-specific band. **b**, **c**, After 24 h Glc depletion, chromatin samples were prepared from HeLa cells treated with 4.5 g l^{-1} Glc for the indicated time. The intensities of the western blotting bands (**b**) were quantified (**c**). **d**, **e**, The effects of OGT knockdown (**d**) or H2B mutations (**e**) on H2B modifications after Glc replenishment. **f**, Western blotting analysis of the H2B modifications in HeLa cells that were cultured in DMEM without Glc (Cont.), or supplemented with 1 mM pyruvate (Pyr.), 10 mM GlcNAc or 4.5 g l^{-1} Glc with or without HBP inhibitors, 6-diazo-5-oxo-L-norleucine (100 μM, DON) or azaserine (100 μM, AZA).

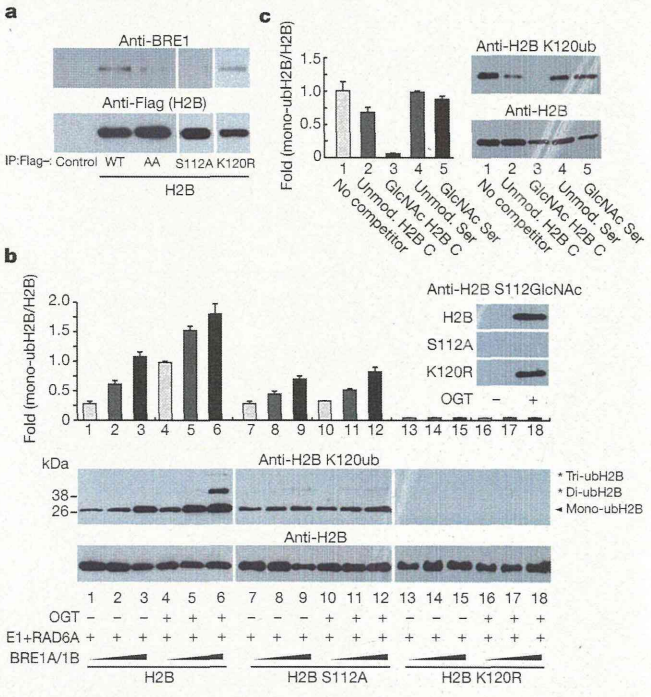

Figure 3 | GlcNAcylation at S112 facilitates ubiquitination at K120 in H2B. **a**, Western blotting analysis of the interaction of H2B mutants with BRE1A. **b**, **c**, *In vitro* monoubiquitination assay with GlcNAcylated H2B (**b**), or in the presence of competitor peptides (**c**). H2B was GlcNAcylated *in vitro* (**b**, top right), and the reactants were subsequently ubiquitinated by H2B monoubiquitination ligase. The reaction was performed with the indicated competitor peptides (0.25 μg ml^{-1}) (**c**). H2B K120 monoubiquitination was detected by western blotting (**b**, bottom; **c**, right) and quantified (**b**, top; **c**, left). Error bars, means and s.d. ($n = 3$).

The terminal GlcNAc of polysaccharides reportedly serves as a recognition moiety for E3 monoubiquitination ligase[16]. Therefore, we proposed that H2B S112 GlcNAc affected K120 monoubiquitination by the BRE1A/1B complex[17]. Flag-tagged H2B, but not AA or S112A, was co-immunoprecipitated with BRE1A (Fig. 3a). This association was observed in the presence of physiological levels of glucose in the media, and BRE1A was bound to H2B S112 GlcNAc (Supplementary Fig. 17). We then assessed how the GlcNAcylation of H2B influenced its *in vitro* ubiquitination by E1, RAD6A (E2) and the BRE1A/1B complex (E3). Although H2B K120 could be substantially ubiquitinated only by the ligases (Supplementary Fig. 18), GlcNAcylation of H2B promoted subsequent H2B ubiquitination, but not its S112A mutant (Fig. 3b). Likewise, ubiquitination was significantly attenuated by the presence of an H2B-S112-GlcNAcylated peptide, but not by either the unmodified control peptide or by GlcNAcylated serine (Fig. 3c). On the basis of these results, we conclude that the GlcNAc moiety at H2B S112 may anchor H2B monoubiquitination ligase.

To illustrate the role of H2B S112 GlcNAc in chromatin regulation, its location was visualized on fly polytene chromosomes. H2B S112 GlcNAc was detected widely in euchromatin, and, as anticipated, its signal disappeared in an OGT-disrupted fly, sxc^{1}/sxc^{78} (Supplementary Fig. 19). H2B S112 GlcNAc overlapped with H3K4 me2 more than with H3K9 me2 or H3K27 me3 (Fig. 4a). Similarly, in immunostained HeLa cells, H2B S112 GlcNAc sites appeared exclusively in 4′,6-diamidino-2-phenylindole (DAPI)-poor areas (Supplementary Fig. 20). Thus, H2B S112 GlcNAc probably accumulates in active chromatin rather than inactive chromatin.

To determine the precise loci of H2B S112 GlcNAc in HeLa cells, we performed chromatin immunoprecipitation (ChIP) and high-throughput sequencing (ChIP-seq). We confirmed ChIP quality by enrichments of H2B GlcNAc as well as H3K4 me2 and H2B K120 monoubiquitination, but neither H3K9 me2 nor H3K27 me3 (Supplementary Fig. 21). A total of 47,375 peaks were found widely distributed over the genome (Supplementary Fig. 22). However, H2B S112 GlcNAc peaked near transcription start sites (TSS), whereas the distribution decreased at transcription termination sites (TTS) (Fig. 4b), suggesting that it correlated with transcriptional regulation. To test this assumption, the activities of genes harbouring H2B S112 GlcNAc near TSS were estimated by microarray analysis (Supplementary Table 2). The average profiles near TSS significantly correlated with gene activity (Fig. 4c). Moreover, the expression levels of the 1,299 genes were reliably measured, and 1,021 genes showed high expression (Supplementary Fig. 23a and Supplementary Table 3b). Moreover, gene ontology analysis revealed that there was an association of the genes harbouring H2B S112 GlcNAc to cellular metabolic processes (Supplementary Fig. 23b and Supplementary Table 3c).

Next, we analysed the genome-wide overlap of H2B S112 GlcNAc with K120 monoubiquitination. A total of 44,158 peaks of H2B K120 monoubiquitination were detected, and their average profiles near TSS were similar to those profiles of H2B S112 GlcNAc (Supplementary

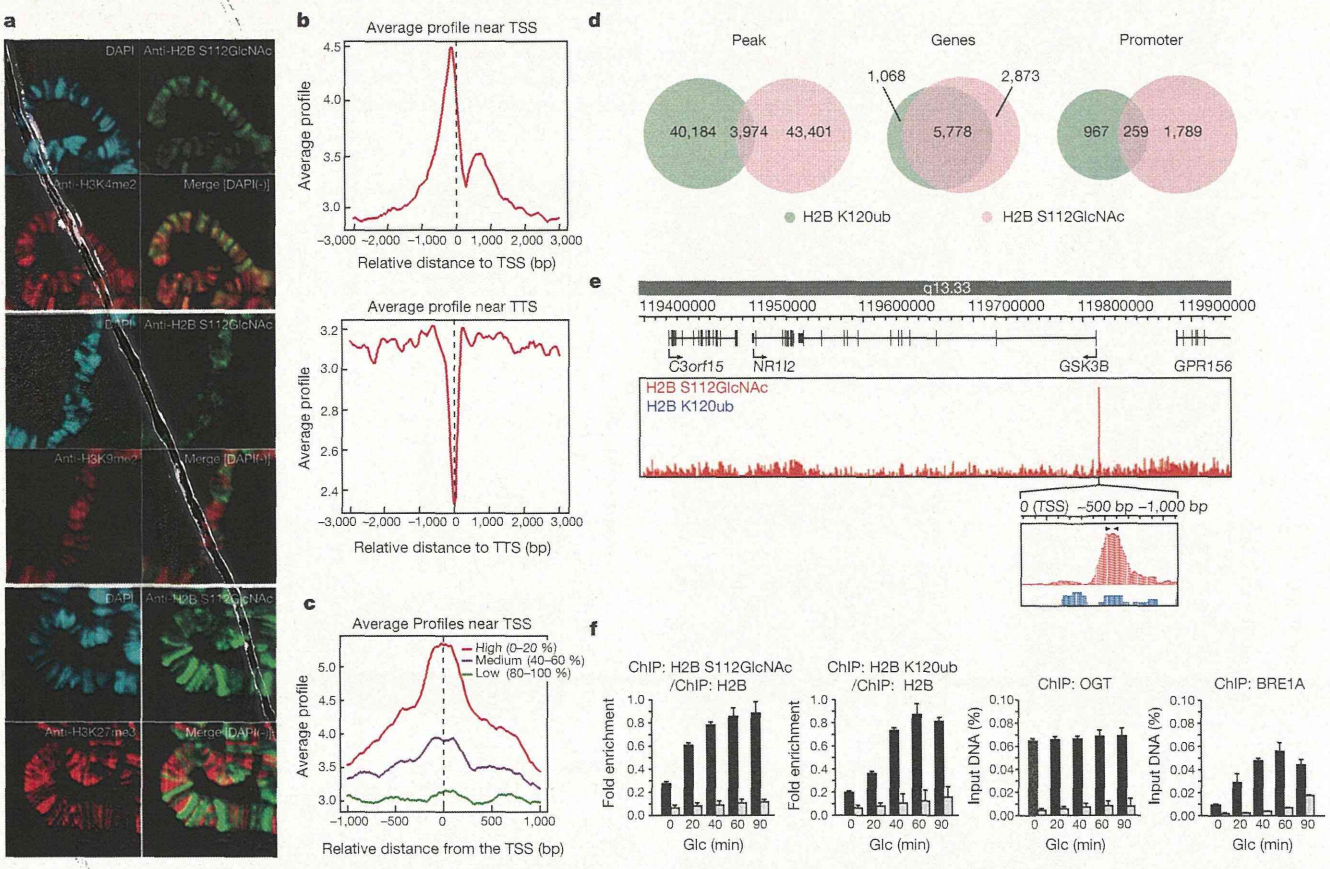

Figure 4 | GlcNAcylated H2B is associated with transcribed genes. **a**, Polytene staining with α-H2B S112 GlcNAc (green) and DAPI (blue) along with α-H3K4me2 (red, top), α-H3K9me2 (red, middle) or α-H3K27me3 (red, bottom). **b–e**, ChIP-seq analysis of the H2B S112 GlcNAc and K120 monoubiquitination. The distributions of H2B S112 GlcNAc were averaged near TSS (top) and TTS (bottom) (**b**). The average profiles of H2B S112 GlcNAc near TSS were calculated based on the associated gene activities (**c**). Venn diagrams showing overlap of the peaks (**d**, left), and the genes (**d**, middle) and the promoter (**d**, right) harbouring the modifications. The ChIP-seq profile surrounding the *GSK3B* gene (**e**). Arrowhead, position of qPCR primer. **f**, ChIP–qPCR validation in the GSK3B promoter. After Glc depletion, the control HeLa cells (black bar) and the OGT-knockdown cells (white bar) were replenished with Glc for 24 h. Then, the cells were subjected to ChIP with the indicated antibody and qPCR analysis. Error bars, means and s.d. ($n = 3$).

Fig. 24). Among the H2B K120 monoubiquitination peaks, nearly 10% (3,974 peaks) overlapped with H2B S112 GlcNAc peaks (Fig. 4d, left), and this evaluation was confirmed by a sequential ChIP–reChIP assay (Supplementary Fig. 25). Although 5,778 genes (66.8% of H2B S112 GlcNAc and 84.4% of K120 monoubiquitination) were found at the same loci (Fig. 4d, middle, and Supplementary Table 3d), 259 genes were identified when the two peaks were compared only within the promoters (Fig. 4d, right). The results of the ChIP-seq analysis were validated by ChIP–quantitative PCR (qPCR) assessment for the glycogen synthase kinase 3β (*GSK3B*) gene (Fig. 4e, f). These findings suggest that at several H2B S112 GlcNAc sites, it aids H2B monoubiquitination ligase recruitment whereas at others additional or different factors may be operational.

Here we provide evidence that histone GlcNAcylation is a post-translational modification correlated with active transcriptional events, and is responsive to serum glucose levels and/or cellular energy states in certain cell types (Supplementary Fig. 1). Using an antibody that specifically recognizes the S112 GlcNAc moiety of endogenous H2B, H2B was shown to serve as an OGT substrate. We have focused on the role of H2B S112 GlcNAcylation in gene regulation (Supplementary Fig. 1). Genome-wide analysis revealed that H2B S112 GlcNAc was frequently located near transcribed genes, suggesting that histone GlcNAcylation facilitates transcription of the genes. This idea is supported by previous reports that transcriptional output driven by several transcription factors is co-activated by OGT[9,18–20]. However, recent papers reported that *Drosophila* OGT is itself a polycomb group protein[8,21], and that many *O*-GlcNAcylated factors are involved in transcriptional repression and gene silencing[7,8]. In this respect, it will be interesting to identify other histone glycosylation sites and investigate their roles in transcriptional repression as well as activation.

METHODS SUMMARY

Plasmids and cell culture. All plasmids were generated with standard protocols (see Methods). Retrovirus production, infection and sorting of the infected cells followed previously reported protocols[9].

Purification of GlcNAc proteins from chromatin. Chromatin pellets were prepared from HeLa cells as previously described[22]. GlcNAc proteins were enriched with α-*O*-GlcNAc (RL2) antibody (Abcam) immobilized on Dynabeads (Invitrogen), and released with GlcNAc-*O*-serine.

Generation of monoclonal antibody. The synthetic H2B S112 GlcNAc peptide (CKHAV S(GlcNAc) EGTK) was used to immunize mice. The hybridomas were selected by enzyme-linked immunosorbent assay (ELISA) and western blotting analysis.

***In vitro* OGT and monoubiquitination assays.** Flag–OGT, Flag–E1, and Flag–BRE1A/BRE1B were purified by baculoviral systems, whereas histones and 6 × His-RAD6A were prepared from bacteria as previously reported[17,23]. H2B was incubated with OGT or H2B monoubiquitination ligases *in vitro*, and its modification was detected by western blotting as previously reported[9,23].

ChIP-seq and ChIP–qPCR. ChIP and ChIP-seq library construction was performed as previously described[24,25], and the libraries were sequenced to 50 base pairs (bp) with Hiseq2000 (Illumina). The fragments of interest in the libraries were quantified with specific promoter sets (Methods) by qPCR.

Full Methods and any associated references are available in the online version of the paper at www.nature.com/nature.

Received 16 July 2010; accepted 20 October 2011.
Published online 27 November 2011.

1. Strahl, B. D. & Allis, C. D. The language of covalent histone modifications. *Nature* **403,** 41–45 (2000).
2. Kouzarides, T. Chromatin modifications and their function. *Cell* **128,** 693–705 (2007).
3. Li, B., Carey, M. & Workman, J. L. The role of chromatin during transcription. *Cell* **128,** 707–719 (2007).
4. Berger, S. L. The complex language of chromatin regulation during transcription. *Nature* **447,** 407–412 (2007).
5. Hart, G. W., Housley, M. P. & Slawson, C. Cycling of O-linked β-*N*-acetylglucosamine on nucleocytoplasmic proteins. *Nature* **446,** 1017–1022 (2007).
6. Love, D. C. & Hanover, J. A. The hexosamine signaling pathway: deciphering the 'O-GlcNAc code'. *Sci. STKE* **2005,** re13 (2005).
7. Yang, X., Zhang, F. & Kudlow, J. E. Recruitment of O-GlcNAc transferase to promoters by corepressor mSin3A: coupling protein O-GlcNAcylation to transcriptional repression. *Cell* **110,** 69–80 (2002).
8. Gambetta, M. C., Oktaba, K. & Muller, J. Essential role of the glycosyltransferase sxc/Ogt in polycomb repression. *Science* **325,** 93–96 (2009).
9. Fujiki, R. *et al.* GlcNAcylation of a histone methyltransferase in retinoic-acid-induced granulopoiesis. *Nature* **459,** 455–459 (2009).
10. Wang, Z. *et al.* Extensive crosstalk between O-GlcNAcylation and phosphorylation regulates cytokinesis. *Sci. Signal.* **3,** ra2 (2010).
11. Sakabe, K., Wang, Z. & Hart, G. W. β-N-acetylglucosamine (O-GlcNAc) is part of the histone code. *Proc. Natl Acad. Sci. USA* **107,** 19915–19920 (2010).
12. Luger, K. *et al.* Crystal structure of the nucleosome core particle at 2.8 Å resolution. *Nature* **389,** 251–260 (1997).
13. Das, C., Lucia, M. S., Hansen, K. C. & Tyler, J. K. CBP/p300-mediated acetylation of histone H3 on lysine 56. *Nature* **459,** 113–117 (2009).
14. Dang, W. *et al.* Histone H4 lysine 16 acetylation regulates cellular lifespan. *Nature* **459,** 802–807 (2009).
15. Dong, L. & Xu, C. W. Carbohydrates induce mono-ubiquitination of H2B in yeast. *J. Biol. Chem.* **279,** 1577–1580 (2004).
16. Yoshida, Y. *et al.* E3 ubiquitin ligase that recognizes sugar chains. *Nature* **418,** 438–442 (2002).
17. Kim, J. *et al.* RAD6-Mediated transcription-coupled H2B ubiquitylation directly stimulates H3K4 methylation in human cells. *Cell* **137,** 459–471 (2009).
18. Dentin, R. *et al.* Hepatic glucose sensing via the CREB coactivator CRTC2. *Science* **319,** 1402–1405 (2008).
19. Chikanishi, T. *et al.* Glucose-induced expression of MIP-1 genes requires O-GlcNAc transferase in monocytes. *Biochem. Biophys. Res. Commun.* **394,** 865–870 (2010).
20. Jackson, S. P. & Tjian, R. O-glycosylation of eukaryotic transcription factors: implications for mechanisms of transcriptional regulation. *Cell* **55,** 125–133 (1988).
21. Sinclair, D. A. *et al. Drosophila* O-GlcNAc transferase (OGT) is encoded by the Polycomb group (PcG) gene, super sex combs (sxc). *Proc. Natl Acad. Sci. USA* **106,** 13427–13432 (2009).
22. Sawatsubashi, S. *et al.* A histone chaperone, DEK, transcriptionally coactivates a nuclear receptor. *Genes Dev.* **24,** 159–170 (2009).
23. Fujiki, R. *et al.* Ligand-induced transrepression by VDR through association of WSTF with acetylated histones. *EMBO J.* **24,** 3881–3894 (2005).
24. He, H. H. *et al.* Nucleosome dynamics define transcriptional enhancers. *Nature Genet.* **42,** 343–347 (2010).
25. Minsky, N. *et al.* Monoubiquitinated H2B is associated with the transcribed region of highly expressed genes in human cells. *Nature Cell Biol.* **10,** 483–488 (2008).

Supplementary Information is linked to the online version of the paper at www.nature.com/nature.

Acknowledgements We thank A. Miyajima, S. Saito and N. Moriyama for experimental support, and M. Yamaki for manuscript preparation. We also thank Y. Maekawa, J. Seta and N. Iwasaki for support with MS. This work was supported in part by The Naito Foundation, the Astellas foundation (to R.F.), the Ministry of Education, Culture, Sports, Science and Technology (MEXT) and the Japan Society for the Promotion of Science (to R.F. and S.K.).

Author Contributions S.K. planned the study with H.K.; R.G.R. and M.B. provided support and general guidance; R.F. designed the study and performed the experiments with H.S. (α-*O*-GlcNAc purification), A.Y. (LC–MS/MS), W.H. (*O*-GlcNAc site mapping), T.C. (*in vitro* OGT assay), S.I. (*Drosophila* analysis), Y.I., H.H.H. (ChIP-seq), F.O., J.K. (*in vitro* monoubiquitination assay), K.I. and J.K (microarray).

Author Information Reprints and permissions information is available at www.nature.com/reprints. The authors declare no competing financial interests. Readers are welcome to comment on the online version of this article at www.nature.com/nature. Correspondence and requests for materials should be addressed to S.K. (uskato@mail.ecc.u-tokyo.ac.jp).

METHODS

Plasmids and retroviruses. Complementary DNAs (cDNAs) of N-terminally Flag-tagged H2B and its mutant were subcloned into pcDNA3 (Invitrogen). A series of H2B point mutants were subcloned into the pET3 vector (Novagen). shRNA sequences targeting hOGT (5′-GCACATAGCAATCTGGCTTCC-3′) and *Renilla* luciferase (5′-TGCGTTGCTAGTACCAAC-3′, as a control) were inserted into the pSIREN-RetroQ-ZsGreen vector (Clontech). For retroviral production, the constructed shRNA vectors were transfected into PLAT-A cells. The virus contained in the medium was used for infection.

Generation of stable cell lines. To generate OGT-KD cells by retroviral infection, 10^6 cells were plated in 60 mm culture dishes, treated with 3 ml of retroviral cocktail (1 ml of the prepared retroviral solution plus 2 ml of DMEM with 10% FBS and 8 μg ml^{-1} polybrene), then cultured for another 48 h. A FACSVantage (BD) sorter was used to isolate the retrovirally transduced, enhanced green fluorescent protein (eGFP)-positive cells, as previously described[9]. To generate the cells stably expressing Flag-tagged constructs, HeLa cells were transfected with the pcDNA vectors encoding the Flag-tagged H2B or the AA mutant. The cells containing the integrated vectors were selected by exposure to 0.5 mg ml^{-1} G418.

Generation of monoclonal antibody. H2B S112 GlcNAc peptide (CKHAV S(GlcNAc) EGTK) was synthesized (MBL Institute) and used as an antigen (Operon Biotechnologies). The hybridomas were briefly screened using ELISA with the GlcNAc peptide, and finally selected by immunoblot analysis with the *in vitro* GlcNAcylated H2B.

Antibodies. Antibodies were obtained as follows: α-Flag M2 agarose (Sigma), α-H2A, α-H2B, α-H3, α-H4 (Abcam), α-H2B K120 monoubiquitination (Upstate), α-GlcNAc (RL2 or CTD110.6) (Abcam), α-OGT (Sigma), α-Flag (Sigma) and α-RNF20/BRE1A (Bethyl).

Purification and identification of GlcNAc proteins. The α-*O*-GlcNAc-immobilized beads were prepared with 15 μg α-*O*-GlcNAc (RL2) antibody and 0.5 ml of Dynabeads M-280 sheep α-mouse IgG (Invitrogen) according to the manufacturer's instructions. Chromatin extracts from HeLa cells (0.5 g protein) were prepared essentially as previously described[22]. In brief, the chromatin pellet, which consisted of residual material from the nuclear extract preparation with buffers supplemented with 1 mM streptozotocin (STZ), was re-suspended with micrococcal nuclease (MNase) buffer (20 mM Tris-HCl, 1 mM $CaCl_2$, 2 mM $MgCl_2$, 0.1 M KCl, 0.1% (v/v) Triton-X, 0.3 M sucrose, 1 mM DTT, 1 mM benzamidine, 0.2 mM PMSF, 1 mM STZ, pH 7.9). After addition of 3 U ml^{-1} MNase, the samples were incubated for 30 min at room temperature with continuous homogenization and the reaction was stopped by adding 5 mM EGTA and 5 mM EDTA. After centrifugation at 2,000*g* for 30 min at 4 °C, the supernatant (chromatin extract) was used for the following purification steps. The chromatin extracts were passed through a WGA agarose column (Vector). The flow-through fraction was further mixed with α-*O*-GlcNAc-immobilized beads and rotated for 8 h at 4 °C. After three washes with buffer D (20 mM Tris-HCl, 0.2 mM EDTA, 5 mM $MgCl_2$, 0.1 M KCl, 0.05% (v/v) NP-40, 10% (v/v) glycerol, 1 mM DTT, 1 mM benzamidine, 0.2 mM PMSF, 1 mM STZ, pH 7.9), glycoproteins were eluted twice with buffer D plus 0.4 mg ml^{-1} GlcNAc-*O*-serine (MBL) (elutions 1 and 2) and finally with 0.1 M glycine-HCl (pH2.0) (elution 3). Eluted proteins were desalted by methanol–chloroform precipitation, digested with trypsin (Promega) then loaded on the automated LC–MS/MS system, which was assembled with Zaplous nano-LC (AMR) plumbed with a reverse-phase C18 electrospray ionization (ESI) column (LC assist) and a Fiinigan LTQ ion-trap mass spectrometer (Thermo). The LC–MS/MS data were processed using Thermo BioWorks (Thermo) and SEQUEST (Thermo) for protein identification. The list of the identified proteins was further analysed by using the 'gene functional classification tool' in DAVID bioinformatics resources 6.7 (http://david.abcc.ncifcrf.gov/).

Recombinant proteins. Preparation of recombinant proteins was performed as previously reported[9,23]. Recombinant Flag–OGT, Flag–E1, Flag–BRE1A/B complexes were isolated by baculovirus expression and immunoprecipitation-based purification with α-Flag M2 agarose (Sigma). Recombinant 6 × His-RAD6A was expressed in bacteria and partly isolated with a HIS-Select Nickel Affinity Gel (Sigma). The eluate was diluted 1:20 with BC0 (20 mM HEPES, 0.2 mM EDTA, 10% (v/v) glycerol, pH 7.9), and fractionated with a Resource Q column (GE Healthcare) using a linear gradient (0–0.5 M KCl) method. Preparation of recombinant *Xenopus* histone H2B and its mutants was performed as previously described[9,23].

***In vitro* GlcNAcylation assay (autoradiographic analysis).** Recombinant Flag–OGT protein (0.5 μg) was incubated with 0.5 μg of recombinant histone and 0.2 mM (0.2 μCi) UDP-[^{3}H]GlcNAc (PerkinElmer) in a 25 μl reaction (50 mM Tris-HCl, 12.5 mM $MgCl_2$, 1 mM DTT, pH 7.5) for 24 h at 37 °C. The reaction was resolved with SDS–PAGE, blotted onto a polyvinylidene difluoride (PVDF) membrane, then subjected to autoradiography after spraying EN^{3}HANCE (NEN Lifescience).

***In vitro* GlcNAcylation assay (MS analysis).** Recombinant histones (1 μg) or recombinant histone octamers assembled *in vitro* (1 μg) were GlcNAcylated by recombinant Flag–OGT in 25 μl reactions (50 mM Tris-HCl, 2 mM UDP-GlcNAc, 12.5 mM $MgCl_2$, 1 mM DTT, pH 7.5) for 24 h at 37 °C. The reactions were directly subjected to a nano-LC ESI–TOF mass spectrometer system, which was assembled with a 1100 nanoLC (Agilent) plumbed with a ZORBAX 300SB-C18 column (Agilent) and micrOTOF (Bruker). Or, the reactions were digested with trypsin (Promega) and subjected to purification of glycopeptides with an MB-LAC WGA kit (Bruker). The enriched glycopeptides were loaded on the nano-LC ESI–ETD ion-trap mass-spectrometer system, which was assembled with the Agilent HP1200 Nano (Agilent) plumbed with ZORBAX 300SB-C18 (Agilent) and amaZon ETD (Bruker).

***In vitro* monoubiquitination assay.** GlcNAcylated histones (1 μg) were ubiquitinated with the E1 (0.1 μg), RAD6 (0.2 μg), BRE1 complex (0.5 μg), ubiquitin (3 μg) in 50 mM Tris (pH7.9), 5 mM $MgCl_2$, 4 mM ATP at 37 °C for 24 h.

ChIP-seq and ChIP–qPCR. ChIP and ChIP-seq libraries were constructed as previously described[24,25]. For ChIP-seq analysis, the libraries were sequenced to 50 bp with Hiseq2000 (Illumina). For ChIP–qPCR analysis, the fragments of interest in the libraries were quantified with Thermal Cycler TP800 (TAKARA) and SYBR Premix Ex Taq II (Takara). The qPCR primer sets for the *GSK3B* gene were 5′-TGCAAGCTCTCAGACGCTAA-3′ and 5′-CTCATTTCTCATGGGCG TTT-3′.